

Low-Cost Force-Sensing Arthroscopic Tool Using Threaded Fiber Bragg Grating Sensors*

Daniel S. Yurkewich, *Student Member, IEEE*, Abelardo Escoto, Ana Luisa Trejos, *Member, IEEE*, Marie-Eve LeBel, Rajni V. Patel, *Life Fellow, IEEE*, Michael D. Naish, *Member, IEEE*

Abstract— Minimally-invasive surgery has revolutionized many medical procedures; however, it also impedes the ability to feel the interaction between the surgical tool and the anatomical part being operated on. In order to address this problem, it is necessary to obtain accurate measurements of the interaction forces exerted on the surgical tools during surgery. These forces can then be manifested to the surgeon via a haptic device or presented visually (visual-force feedback). This paper describes the use of a fiber optic device to measure and display to the surgeon interaction forces acting on an arthroscopic tool. The sensorization of the tool involves a simple, highly efficient and robust design and is ideally suited for use in a surgical training environment aimed at narrowing the gap between trainees and expert surgeons before the trainees proceed to their first surgery *in vivo*. The major advantages of using fiber optics include their small size, their local simplicity, their ease of sterilization, and their high sensitivity. In this paper, a complete low-cost sensing solution is described, including 1) fiber Bragg grating sensors, 2) high resolution electronic signal processing, 3) fabrication of the tool using a wire electrical discharge machine (EDM) and 3D metal sintering technologies. Experimental results demonstrate the accuracy and performance of the sensorized tool.

I. INTRODUCTION

Minimally-invasive surgery (MIS) has become a widely accepted alternative to open surgery in a broad number of surgical specialties. Certain orthopaedic procedures, such as meniscectomies and ligament reconstructions [1,2], are now mostly performed arthroscopically. There are many benefits of using small access points as opposed to the large incisions used in open surgeries. These include, but are not limited to, better cosmesis [3], reduced blood loss [4,5], less pain [4], reduced infection rates [6,7], faster recovery and shorter hospital stay [5]. The major hindrances in MIS, however, are reduced tactile feedback [8,9] and a steep learning curve

[10]. While expert surgeons have risen to this challenge through deliberate practice, the novice surgeon or trainee has limited opportunities to practice their skills before operating on their first patient. In the last decade, multiple simulators have been developed to address this problem, but the simulated haptic feedback is not always representative of the real surgical situations. Therefore, the development of force-sensing arthroscopic instruments may assist in training novice orthopaedic surgeons, as well as allow for surgical force data to be collected for both novices and experts. This data may prove useful for the objective assessment of surgical skill.

A. Fiber Optic Technology

The use of fiber optic technology has become more prevalent as its potential has been explored. The thin diameter of optical fibers makes it well-suited to smaller diameter tools; the sensitivity of the sensor is increased; the signal-to-noise ratio is minimized; and their composition allows for magnetic resonance imaging (MRI) usability and biocompatibility. The presented arthroscopic force sensing design uses fiber Bragg grating (FBG) sensors fabricated with UV light imprinting. These sensors have already emerged in a multitude of medical applications [11] due to their relatively simple adhesion and alignment, their high sensitivity [12,13], and their internal sensing property. The theoretical strain values can be determined using an optical spectrum analyzer and Bragg wavelength equations [14], or by using a low-cost system that produces a calibration curve between applied strain and refracted light.

B. Force Sensing

Force sensing feedback can indicate if the surgeon is applying the right amount of force to an area within the surgical site. In orthopaedic surgery, since contact can occur between either soft tissue or bone, tactile force feedback can augment the image from the arthroscope to help characterize the stiffness of the tissue in contact with the instrument, and to gauge the appropriate forces to apply. In a related paper by Trejos *et al.* [15], a laparoscopic instrument was developed to measure all degrees of freedom acting on the instrument during surgery. With particular focus on FBG sensorized tools, Piers *et al.* [16] designed a 5 mm diameter tri-axial 3-fiber tool that functioned as a Fabry-Pérot device, measuring the ratio of the reflected light from a 100 μm distal flat mirror and the polished fiber end. A similar Fabry-Pérot device was created by Liu *et al.* [17] to outfit a probe for vitreoretinal microsurgery. He *et al.* [18] developed a

* This research was supported by the Natural Sciences and Engineering Research Council (NSERC) of Canada under grants RGPIN-1345 and 312393-2010; by the Ontario Research Fund—Research Excellence Grant RE-05-049, and by infrastructure grants from the Canada Foundation for Innovation awarded to the London Health Sciences Centre (Canadian Surgical Technologies & Advanced Robotics (CSTAR)). D.S. Yurkewich is with CSTAR and with the Dept. of Electrical and Computer Engineering (ECE), Western University (Western) (email: dyurkewi@gmail.com). A. Escoto is with CSTAR (email: abescoto@gmail.com). A.L. Trejos is with CSTAR and ECE, Western (email: atrejos@uwo.ca). R.V. Patel is with CSTAR, ECE and the Dept. of Surgery, Western (email: rvpatel@uwo.ca). M.-E. LeBel is with CSTAR and the Division of Orthopaedic Surgery, Western (email: mlebel4@uwo.ca). M.D. Naish is with CSTAR, the Dept. of Mechanical and Materials Engineering and ECE, Western (email: mnaish@uwo.ca).

miniaturized FBG vitreoretinal grasper capable of sensing forces imperceptible to human touch.

C. Motivation and Objectives

The goal of this work was to design a robust, sterilizable arthroscopic grasper that can measure the forces acting on it during use. While many instruments feature small size, high sensitivity/resolution, and biocompatibility, no existing tool demonstrates all of these features in a contained, surgery-ready, aesthetic grasper design using FBGs. With insertion into a minimally invasive hole or trocar, the movement of the tool is restricted to both axial translation, and rotation around the entry point in 3 axes. The tool also contains an added degree of freedom for actuation of the grasping jaws.

The MIS tool was developed with the following list of design constraints: (i) diameter less than 5 mm; (ii) force sensitivity of 1/10 N; (iii) 0 to 20 N grasping force; (iv) tip lateral forces measurable between -10 and 10 N applied 360 degrees around the tool; (v) yielding failure before fracture; (vi) biocompatible, sterilizable, high temperature resistance, chemically-inert; (vii) aesthetic and dimensionally equal to current tools; (viii) low-friction motion of grasper handle and jaws; (ix) smoothed corners to minimize tissue catching. The current grasper design measures x and y bending forces, and grasping force. Axial (z) force (prodding/pulling) will be incorporated in the next generation of this design.

II. LOW-COST FIBER OPTIC INTERROGATION UNIT

A. State of the Art

As the potential of fiber Bragg gratings has been realized, several researchers have investigated the benefits of creating an all-fiber interrogation unit in order to reduce cost and increase signal quality. Tosi *et al.* [19] have introduced an in-line sensing system to test the lowest cost system that can still give a good signal. By using an intricate method of signal processing, the \$1k setup made up of a laser, isolator, inline FBGs, photodiodes, and a conditioning unit gives accuracy to the 10 nε level, which compares to systems estimated to cost \$10k to \$100k. An all-fiber sensing system created by Davis *et al.* [20] uses a broadband source in conjunction with a wavelength division coupler to interrogate the gratings and returns a finer spectrum. In the application of minimally invasive tools, the temperature dependency of FBGs can skew the results when the tool is inserted into the body. One solution to this dilemma is presented by Wu *et al.* [21], where a reference sensor is used in combination with parallel photodiodes to ratiometrically reduce the effect of temperature.

B. Current Design

The fiber optic interrogation system used for the results in this paper was designed as an all-fiber unit (Fig. 1), decreasing the total interrogation system cost from approximately \$25,000 CAD with an interrogator to \$4,650 CAD, while still maintaining the signal constraints. The figure shows the interrogation of one sensor (of four) through a photodiode (PD), signal processing circuit board (SP) and then to a user interface with force readout on a PC.

A single-mode benchtop super luminescent diode (SLD) source (S5FC1005S, ThorLabs) was used to provide the system with 1550 nm (45 nm BW) light at 22 mW. The SLD was directly connected to one of nine 1550 nm circulators (New Focus Inc.) that interrogated the 1544 nm reference fiber. The reference fiber (os1100, MicronOptics), along with the other 8 available sensor fibers, was inscribed with a 1544 nm fiber Bragg grating (FBG). The refracted light from this grating was input to a 1×8 fiber optic coupler (F-CPL-1X8-OPT, Newport) to potentially power an 8 fiber sensing system (8 DOF). By attaching the reference fiber before the splitter, only one reference fiber was needed. From the 1×8 coupler, the light is sent through separate circulators directly to the sensing fiber (Port 2). By using the reflected light instead of the transmitted light as the measurand, the fiber Bragg grating could be placed very close to the tip of the tool. The refracted light (through Port 3) was directly connected by SC-SC connectors to the photodiodes of the electrical system.

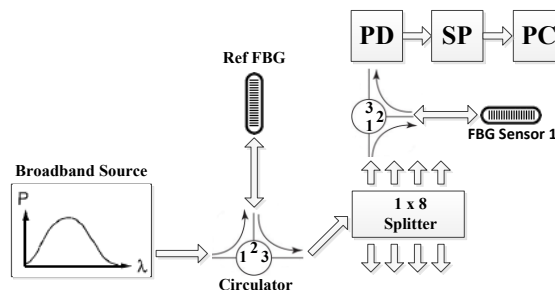


Figure 1. Fiber optic instrumentation schematic.

III. ELECTRICAL SIGNAL PROCESSING

At the optic-electronic interface of the system, 8 high-sensitivity optical fiber InGaAs photodiodes (ETX100, JDSU) are used at a 1550 nm frequency to transform the light into current. A transimpedance amplifier (OPA381AIDGKT, Texas Instruments) was used after each photodiode to amplify the current rather than the nonlinear impedance. A very low noise 24-bit Analog-to-Digital Converter (ADC) (ADS1256, Texas Instruments) was then used to transform the analog signal into a 24-bit digital signal. A microcontroller (PIC16F690, Microchip) was used to initialize the ADC, poll for and merge the 24-bit data, and synchronize data transmission, thereby ensuring reliable data transfer. There was a tradeoff between frequency and bit resolution. The final ADC specifications used included a 10 N range with a resolution of 0.1 mN, equating to 18.91 noise-free bits. This provided a theoretical sample rate of 1000 samples per second, equivalent to 75 Hz for 4 fibers.

IV. TOOL DESIGN AND MANUFACTURING

The primary challenge in making the tool was to design for accurate sensor placement, adhesion, and containment, while considering tool deformation, friction, and biocompatibility. With small overall tool size being an important objective, further challenges were faced while designing the small tool components for compatibility and

machinability. Additionally, the presented tool allows all of the components to come apart safely to effectively clean and sterilize each component.

The manufactured grasper shown in Fig. 2 is based on the 011024 ACUFEX “Alligator Max” arthroscopic grasper. The diameter of the new tool is 4.57 mm, and the length from handle to grasper tip is 17 cm. The major change to this design includes a concentric slotted tube shaft design to protect the sensors from physical contact and bio-exposure.



Figure 2. Full arthroscopic grasper with 3 extruding fibers.

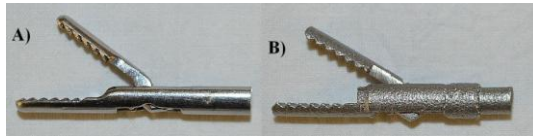


Figure 3. A) Cut ACUFEX jaws B) Sintered jaws.

Grasper Jaws—The most complex geometry in the grasper is the grasping jaws (Fig. 3). The proximal end of the grasper jaws was given a double-stepped design to fit both the small sensor shaft, and the larger covering shaft, allowing the jaws to be easily removed. The parts were produced on a 3-D sintering system (DM 125, 3D Systems) in stainless steel.

Slotted Fiber Guides—Three slots, for three 200 μm diameter fibers spaced 120° apart, were eroded into a 380 μm thick 4.19 mm OD hypodermic tube (304H08RW, MicroGroup) using a wire-EDM machine. A larger hypodermic tube (304H07X, MicroGroup) is used to cover the sensor shaft and protect the fibers from the environment. The fibers curve back at the proximal end of the shaft to safely connect to a stress-relief boot at the tool exit (Fig. 4).

Handles and Actuating Rod—CNC and wire-EDM systems were used to fabricate the handles and actuating rod. A medical grade finish was applied through a combination of grinding, sanding, and glass-bead blasting to increase the grasper aesthetics, ergonomics, and biocompatibility (Fig. 5).

V. SENSOR CALIBRATION

A. Sensor Shaft Calibration (Axial)

The four sensors on the tool are capable of measuring x , y lateral, and z axial forces at the tip (3 sensors), as well as measuring tip grasping force (1 sensor). Under axial loading between ± 20 N within an axial test jig, the tool began to deflect in bending (as concluded from the sensor readings), before showing a change in force that signaled tool extension or compression. A pure axial load is indicated by the signal dropping (compression) or rising (extension) amongst all

three sensor signals; however, this was not seen, and so a resultant axial force could not be obtained. This result indicates that the grasper sensor shaft does not have large enough axial deformation to bending sensitivity ratio to read all of the loading combinations distinctly. The testing jig consisted of an ATI Nano 43 force/torque sensor attached to a Zaber Tech linear stage. The handle was fixed to a base, while the jaws were set into a jaw-shaped plastic complement attached to the force sensor. Incremental steps of the linear stage gave readings on the fiber optic sensors and ATI sensor simultaneously to determine the force-strain relationship.

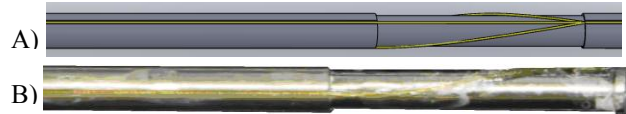


Figure 4. A) SolidWorks model of fiber guides B) Actual instrument.

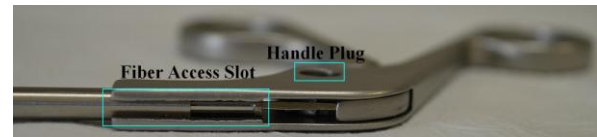


Figure 5. Grasper assembly view.



Figure 6. Bending calibration apparatus.

B. Sensor Shaft Calibration (Bending)

Since the axial sensitivity was too low, the third shaft sensor was instead used in bending calibration to average out the errors between the other two shaft sensors. In future tool generations, this fiber will be used to measure the axial force of the instrument. The 1 cm grating in each of the fibers stretches from 3 cm to 4 cm from the tool tip. The importance of adding the sensor gratings close to the instrument tip is to eliminate any external forces caused by interaction with the trocar/entry port. The x and y tool forces were measured by hanging weights from 0 to 500 g in 100 g increments in each direction on the second tooth of the lower grasper jaw in a cantilever configuration (Fig. 6). The support point was located 1 cm from the shaft-handle connection, for a cantilever arm length of 13.25 cm. The tool was rotated manually in 60-degree intervals for a total of six positional measurements within a calibration jig. The signals from each of the three fiber sensors were recorded at each weight and position. This process was repeated 8 times to give a total of 480 readings per fiber.

Reference curves were chosen for sensor calibration, due to theoretical uncertainties in grating precision, location, spectrum shape, and power loss. The calibration curves for the three fibers from -5 N to 5 N can be seen in Fig. 7, where the vertical axis represents the FBG voltage output of each

signal. The nonlinearity in the graphs is caused by the parabolic shape of the FBG spectrum. Eleven readings were taken while each sensor was in maximal tension (inline with the applied load) or maximal compression (180° from the applied load) over the 10 N range to formulate the three calibration curves.

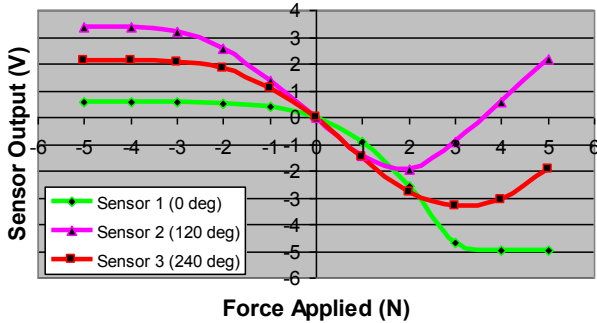


Figure 7. FBG calibration curves.

C. Grasper Calibration

The grasping force FBG sensor was placed on the 2.5 mm thick stainless steel member of the moving grasper handle, approximately 2.5 cm from the load point of the surgeon’s index or middle finger and 4 cm from the handle fulcrum. As the grasper moving handle is in a direct 4 bar linkage with the moving grasper jaw through the actuating rod, this sensor position was ideal for a grasping force relationship, and was not coupled to any other forces on the grasper tip. The friction within this linkage was minimized through additional filing and sanding until the force of gravity on the moving handle could actuate the jaws alone. For calibration, the grasper jaw tips were secured on a two-plate rapid-prototyped plastic jig with each plate fastened to either side of an ATI Nano 43 force/torque sensor (Fig. 8).

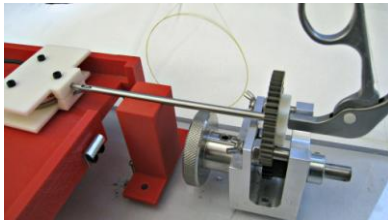


Figure 8. Grasper calibration apparatus.

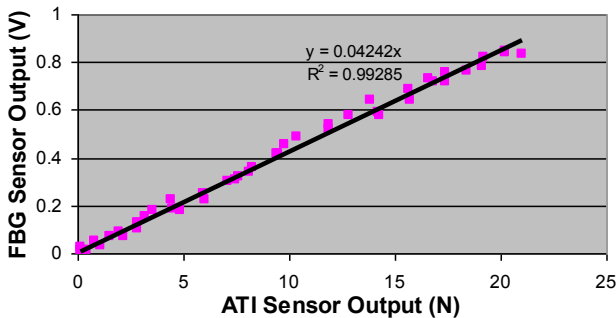


Figure 9. Grasper force calibration.

Force was applied normally to the movable grasper handle while two fixed mounts secured the rest of the tool.

To formulate the calibration line, 44 FBG sensor and F/T sensor outputs were recorded simultaneously between 0 and 20 N in 6 increasing and decreasing loading cycles (Fig. 9).

VI. ASSESSMENT METHODS

To assess the sensing performance of the final prototype, the total resultant tip force measurement and an angle approximation of the direction of the applied load referenced to a vertical axis (Force Angle) were measured for the sensor shaft. For the actuation force, the total force applied by the jaws was measured. The performance of the FBG sensors was assessed based on the following measurements, and formulated in Table I:

i) Accuracy: The root-mean-squared (RMS) error of the shaft sensors was determined from 469 additional readings by again hanging weights from 0 to 500 g in 100 g increments in each direction. The voltages from the 3 fibers were taken and equated to predict the corresponding zero strain neutral axis (NA) as displayed in Fig. 10. Both the total applied force, and the angle of the applied force, referenced vertically down from the top of the instrument (0°), were calculated from these values based on the calibration curves. The RMS error of the grasping force was determined by again applying increasing and decreasing forces to the handle over the range of 0 to 20 N. 76 sensor readings from 6 iterations were used for grasper force prediction measurements based on the grasper calibration line and compared to the readings from the ATI sensor.

ii) Repeatability: The maximum standard deviation (σ) was evaluated for the sensor shaft in 8 repetitions using the same method described above for accuracy. Six loading cycles were performed to assess the repeatability of the grasping force from 0 to 20 N.

iii) Hysteresis: The RMS error was calculated between the increasing and decreasing load values of both the sensor shaft and the grasping sensor using the same data obtained in the accuracy assessment.

iv) Signal Drift and Noise: The signal drift was evaluated after 10 minutes under both a 0 N and a 1 N load. The maximum signal noise was evaluated after 30 seconds per fiber. Both tests were conducted in the linear range of the FBG sensor for consistent results. A 10-minute drift time was chosen to simulate the maximum continuous time in contact with tissue. The auto-biasing method described in Section VII.D will compensate for drift when not in contact.

v) Sensitivity: The minimum sensitivity of the sensors in their linear range was tested by applying force to the grasper tip and grasper handle until the signal was visually discernable from the noise.

vi) Resolution: The maximum effective resolution for this system is limited by the Analog-to-Digital Converter which gives a 20 bit noise-free signal at the 10 Hz 4-fiber frequency (the minimum frequency estimated for effective visual feedback). The resolution was distributed over a ± 5 N load range.

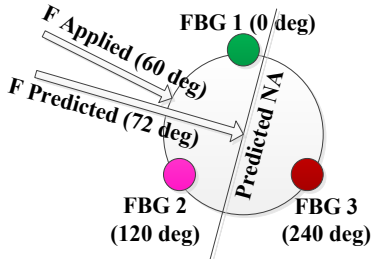


Figure 10. Force and angle prediction at 60 degree applied load.

TABLE I
FBG SENSOR CALIBRATION ASSESSMENT

	RMS error	Max σ	Hysteresis	Noise / Drift
Tip Force (N)	0.213	0.169	0.133	0.075 / -- ¹
Force Angle (°)	4.37	3.87	5.65	0.075 / -- ¹
Actuation (N)	0.747	0.804	3.54	0.075 / -- ¹

¹ No discernable drift

VII. RESULTS AND DISCUSSION

A. Sensor Shaft

The measurements taken from the three fibers at each of the 60° increments were tabulated and equated based on their corresponding locations to give a maximum resultant force and an angle of force application. Fig. 11 shows the relation of the lateral forces compared to angle of tool rotation. Three paired combinations of the three sensors (1–2, 1–3, 2–3) were evaluated. The RMS error in the average force prediction was 0.213 N (unnormalized). The error in the averaged angle prediction was 4.37°. These values are predicted to be suitable for surgical applications, however future *in vivo* testing will confirm applicability.

An ideal case was also considered, where the sensor pair with the lowest error in each case was used for calculating the overall error. This resulted in average force and angle prediction RMS errors of 0.023 N and 3.87°. This result points out the high precision that is possible with these sensors. The most accurate fiber pair was Fibers 2–3, which solely predicted an unnormalized force RMS error of 0.345 N and an angle RMS error of 5.25°. If Sensor 1 is to be used for axial sensing in future designs, this result shows that the remaining 2 fibers will provide high accuracy by themselves. Further improvements in fiber placement, angle measurement, and weight application, will help to reduce errors further and reduce dissimilarities between fibers. The calibration curve was also made with a least-energy spline method to join the discontinuous sample points: additional points for this curve could give more accurate results.

It is important to note that the linear range of the fiber sensors in the sensor shaft calibration curves (see Fig. 7) only extends for approximately 5 N over the 10 N loading range. Also, as the applied forces get larger in Sensors 2 and 3, the uniqueness of the sensor output data dissolves. To address both of these issues, the tool should be made stiffer in order to extend the linear output of the tool strain in both loading directions. While this change will, alone, slightly decrease sensitivity, improvements in signal processing will help counteract this effect. Additionally, for best results, all of the sensors should be pre-strained in a way that the center of their linear region is approximately at the zero loading

condition. Further methods should be developed to accurately pre-strain the fibers on the sensor shaft. In contrast, resolution is maximized and noise is minimized over the ± 2.5 N load span with the narrow linear region. For tests that only require forces in this range, this setup is ideal. As the loading range increases, resolution will slightly decrease and electrical noise will have a more significant impact.

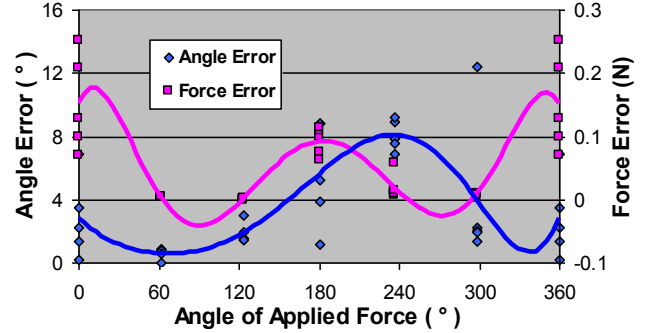


Figure 11. Accuracy errors vs. angle of applied force

B. Grasping

The grasping force sensor was initially placed on the thin actuating rod to achieve a relation between its bending deformation and the grasping force; however, there was too much coupling with the lateral bending of the grasper shaft. By placing the sensor on the grasper handle, the sensor was easily accessible for calibration, and was not coupled to lateral tip forces. It could also be pre-strained accurately such that a 20 N grasping load was measurable within the linear region of the grasping FBG sensor. The RMS accuracy error in this load range was 0.747 N, further decomposed into a 0.663 N error for 0–10 N and 0.830 N error for 10–20 N. Due to loose joints in the system, and to large bending of the thin actuating rod, there was significant hysteresis error between force application and relaxation in the results. Future designs will therefore incorporate a more rigid actuating rod, and tighter tolerance components.

C. Overall System Performance

Minimal processing was applied to the signal because the signal to noise ratio was already initially high with a 0.075 N noise error and a negligible drift error. Since fiber optic sensors are not prone to electrical noise, and the light noise was insignificant to the broadband power, all of the noise is assumed to be within the circuit board design. Furthermore, with additional circuit board design considerations, the ADC resolution potential can be increased by 2.63 times from the current resolution of 0.01 mN. The use of low-cost “quick-connect” SC connectors versus fusion splicing also produced noise via alignment issues with the FBGs, the splitter, the circulators, and the broadband power supply. The current recorded sensitivity of the fibers is approximately 0.05 N.

D. Auto Zero-Drift Compensation Method

Due to the low signal noise, and relatively high sensitivity in FBGs, a tested method to calibrate system drift

is to auto-reset the reference zero value if the tool has been under zero load for approximately 3 seconds. With the maximum noise of the system calculated as 0.075 N, a zero load condition is met if the noise remains under 0.1 N for 3 seconds. Further testing on this drift compensation method is recommended to prevent zeroing errors, and to fine tune the zero load period and acceptable load error.

VIII. CONCLUSIONS AND FUTURE WORK

Arthroscopic graspers are precise small-scale devices and providing them with force-sensing capabilities at a low-cost was a challenge. The system is portable and compact, with 2 DOF tip forces, and 1 DOF grasping force. A low-cost system (\$4,650 CAD vs. \$25,000 CAD) was successfully created while obtaining and maintaining good quantitative results. This work will advance MIS training and skills assessment by showing both the novice and the mentoring surgeons how much force is applied to the tissues when reduced or no haptic feedback is available. The instruments will also be tested in real surgeries to analyze the absolute accuracy, resolution and sensitivity required to improve surgical procedures. These tests will also characterize any sensor fluctuations due to changing temperature.

Since the success in implementing the sensing method and design have been demonstrated in an arthroscopic grasper, manufacturing an equivalent sensing shaver and probe is a logical next step. For the next generation grasper, axial force will be added to the instrument to increase the capability of the tool to sense tissue pulling. A conceptual design for the axial stress element to increase axial sensitivity is shown below in Fig. 12. By adding slots with a wire-EDM at 30 degree intervals in 90 degree pairs over a 3 cm length, the sensor shaft will deform 1.419 μm , and the axial sensitivity vs. bending sensitivity will be increased theoretically by 5.42 times (SolidWorks Simulation). The evenly-spaced slots around the circumference of the shaft uniformly increase the bending sensitivity and limit twist. Axial coupling errors for the grasping force sensor, and errors from twisting forces, will be analyzed with the addition of the axial element.

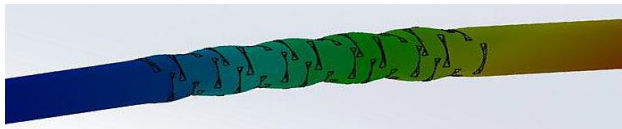


Figure 12. Axial amplification element.

ACKNOWLEDGMENTS

Special thanks goes to colleagues at CSTAR, and to Eugen Porter for electrical instrumentation, Chris Vandelaar for machining and fabrication, Daniele Tosi for fiber optic design, and Aaron Yurkewich for guidance and motivation.

REFERENCES

[1] J. Lozano, C. B. Ma, and W. D. Cannon, "All-inside meniscus repair: a systematic review," *Clinical Orthopaedics and Related Research*, no. 455, pp. 134–141, 2007.

[2] S. E. Cameron, W. Wilson, and P. St. Pierre, "A prospective, randomized comparison of open vs. arthroscopically assisted ACL reconstruction," *Orthopedics*, vol. 18, no. 3, pp. 249–252, 1995.

[3] M. Ohgami, S. Ishii, Y. Arisawa, T. Ohmori, K. Noga, T. Furukawa, and M. Kitajima, "Scarless endoscopic thyroidectomy: breast approach for better cosmesis," *Surgical Laparoscopy, Endoscopy & Percutaneous Techniques*, vol. 10, no. 1, pp. 1–4, February 2000.

[4] P. Modi, A. Hassan, W. R. Chitwood Jr., "Minimally invasive mitral valve surgery: a systematic review and meta-analysis," *European Journal of Cardio-thoracic Surgery*, vol. 34, pp. 943–952, 2008.

[5] Y. Kitagawa, S. Kitano, T. Kubota, K. Kumai, Y. Otani, Y. Saikawa, M. Yoshida, and M. Kitajima, "Minimally invasive surgery for gastric cancer — toward a confluence of two major streams: a review," *Gastric Cancer*, vol. 8, pp. 103–110, 2005.

[6] P. J. Kregor, J. A. Stannard, M. Zlowodzki, and P. A. Cole, "Treatment of distal femur fractures using the less invasive—stabilization system surgical experience and early clinical results in 103 fractures," *J. Orthopedic Trauma*, vol. 18, no. 8, pp. 509–520, 2004.

[7] J. E. O'Toole, K. M. Eichholz, and R. G. Fessler, "Surgical site infection rates after minimally invasive spinal surgery," *Journal of Neurosurgery: Spine*, vol. 11, no. 4, pp. 471–476, 2009.

[8] M. V. Ottermo, M. Øvstedal, T. Langø, Ø. Stavdahl, Y. Yavuz, T. A. Johansen, R. Mårvik, "The Role of Tactile Feedback in Laparoscopic Surgery," *Surgical Laparoscopy, Endoscopy & Percutaneous Techniques*, vol. 16, no. 6, pp. 390–400, 2006.

[9] M.E.H. Eltaib, J.R. Hewit, "Tactile sensing technology for minimal access surgery—a review," *Mechatronics*, vol. 13, pp. 1163–1177, 2003.

[10] V. R. Patel, A. S. Tully, R. Holmes and J. Lindsay, "Robotic radical prostatectomy in the community setting—the learning curve and beyond: initial 200 cases," *J. Urology*, vol. 174, pp. 269–272, 2005.

[11] V. Mishra, N. Singh, U. Tiwari, and P. Kapur, "Fiber grating sensors in medicine: Current and emerging applications," *Sensors and Actuators A: Physical*, vol. 167, no. 2, pp. 279–290, 2011.

[12] C. W. Lai, Y. L. Lo, J. P. Yur, W. F. Liu, and C. H. Chuang, "Application of Fabry-Pérot and fiber Bragg grating pressure sensors to simultaneous measurement of liquid level and specific gravity," *Measurement*, vol. 45, pp. 469–473, 2012.

[13] A. R. Bahrapour, S. Tofghi, M. Bathaee, and F. Farman, "Optical fiber interferometers and their applications," *Interferometry—Research and Applications in Science and Technology*, vol. 1, pp. 3–30, 2012.

[14] M. A. Davis, A. D. Kersey, H. J. Patrick, M. LeBlanc, K. P. Koo, C. G. Askins, M. A. Putnam, and E. J. Friebale, "Fiber grating sensors," *Journal of Lightwave Technology*, vol. 15, no. 8, pp. 1442–63, 1997.

[15] A. L. Trejos, A. C. Lyle, A. Escoto, M. D. Naish, and R. V. Patel, "Force/position-based modular system for minimally invasive surgery," *IEEE Int. Conf. on Robotics and Automation*, Anchorage, AK, May 3–8, 2010, pp. 3660–3665.

[16] J. Piers, J. Clijnen, D. Reynaerts, H. Van Brussel, P. Herijgers, B. Corteville, and S. Boone, "A micro optical force sensor for force feedback during minimally invasive robotic surgery," *Sensors and Actuators A*, vol. 115, pp. 447–455, 2004.

[17] X. Liu, I. I. Iordachita, X. He, R. H. Taylor, and J. U. Kang, "Miniature fiber-optic force sensor for vitreoretinal microsurgery based on low-coherence Fabry-Pérot interferometry," *Proc. SPIE Optical Fibers and Sensors V*, vol. 8218, no. 00, pp. 1–6, 2012.

[18] X. He, J. T. Handa, P. L. Gehlbach, R. H. Taylor, and I. I. Iordachita, "A Submillimetric 3-DOF Force Sensing Instrument With Integrated Fiber Bragg Grating for Retinal Microsurgery," *IEEE Transactions on Biomedical Engineering*, vol. 61, no. 2, pp. 522–534, 2014.

[19] D. Tosi, M. Olivero, G. Perrone, and A. Vallan, "Improved fibre Bragg grating interrogation for dynamic strain measurement," *Deutsche gesellschaft für angewandte optik*, Torino, Corso Duca degli Abruzzi, 2009.

[20] M. A. Davis, and A. D. Kersey, "All-fibre Bragg grating strain-sensor demodulation technique using a wavelength division coupler," *Electronics Letters*, vol. 30, no. 1, pp. 75–77, 1994.

[21] Q. Wu, Y. Semenova, A. Sun, P. Wang, and G. Farrell, "High resolution temperature insensitive interrogation technique for FBG sensors," *Optics and Laser Technology*, vol. 42, no. 4, pp. 653–656, 2009.